Coseismic Displacement of M7.9 Sichuan Earthquake Derived by ALOS Radar Interferometry

Xiaopeng Tong (xitong@ucsd.edu), **David Sandwell, Yuri Fialko**
Scripps Institution of Oceanography, La Jolla, CA

Rob Mellors
San Diego State University, San Diego, CA

Abstract

On May 12th 2008, a major (Mw 7.9) earthquake struck Wenchuan County, Sichuan Province in China. The casualities include approximately 70,000 dead and 374,000 injured. The rupture accompanying the events extends over 270 km toward the northeast, and is a result of the convergent tectonic movement associated with Longmen Shan fault.

We assemble and process ALOS PALSAR data including 6 ascending tracks (> 72 scenes) to map the coseismic displacement with a full coverage of 400 km by 400 km of the fault zone. Mosaicking the 6 tracks requires careful treatment of the precise orbits as well as a new correction for the ionospheric delay which is typically 10 cm ramp in the range direction. Severe ionospheric disturbances cause azimuth pixel shifts which mask the shifts due to the coseismic displacement. Besides, we are developing methods to perform ScanSAR interferometry along the descending track to obtain another independent component of deformation. Interferograms show a large area of decorrelation that coincides with the region of landslides and intensive ground shaking, mostly on the hanging wall of Beichuan faults. We present preliminary results of linear inversions based on the InSAR data. The elastic half space model allows for spatially variable rake angles and illustrates relative contributions of the thrust and strike-slip motion in the deeper part of the fault, as well as the along-strike variability. The surface horizontal motion from GPS observations indicates less strike-slip component than our model. The inferred slip distribution will be used to drive models of postseismic relaxation, which will be compared to InSAR data collected after the earthquake to constrain the relaxation mechanisms, effective rheology, and provide insights into time-dependent stress transfer and future seismic hazard.

New ScanSAR to ScanSAR Interferometry - Descending Orbits

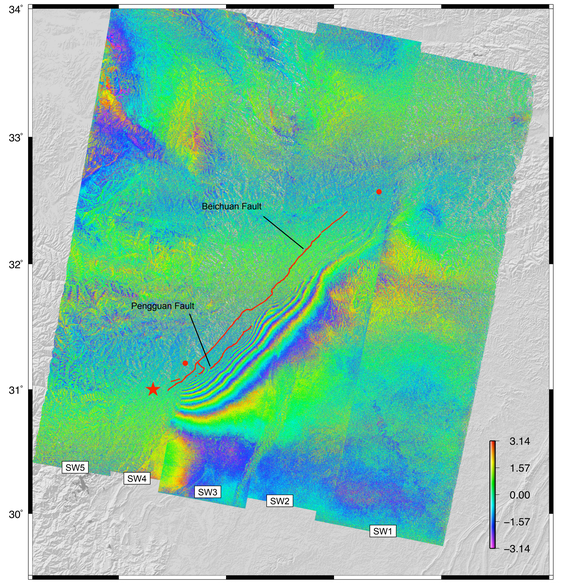

Fig1. Descending ScanSAR to ScanSAR linterferogram (11.8 cm per fringe) from ALOS PALSAR data acquisitions on January 3, 2008 and May 20, 2008. The red star is the main shock, the red circles are the magnitude 6 aftershocks on May 12th and May 25th. The red line is the surface rupture mapped by Jing Liu from the Chinese Academy of Sciences. The total interferogram is constructed from the 5 subswaths (SW1-5). Although the along-track burst alignment of the subswaths is good (78% overlap), the perpendicular baseline is rather long (890 m). The long baseline results in complete decorrelation in the mountain areas because the SRTM 90-m topography is inadequate for accurate phase removal. Nevertheless our modeling (Fig 3, Fig 4, Fig 5) shows that having even a partial phase recovery from a second look direction is important for establishing the partitioning between strike-slip and dip-slip along this major rupture.

ScanSAR to ScanSAR Interferometry

We have developed the computer code to generate interferograms from ALOS ScanSAR data having 5 subswaths. We follow the approach of Balmer and Eineder [1998] where raw data are separated into subswaths and data voids between bursts are filled with zero. The data are then processed using a standard strip-mode processor. In addition to having a short baseline and adequate Doppler overlap, the pulse repetition frequencies of the reference and repeat images must match and the bursts must have more than 30% overlap. Data over Los Angeles were used for developing FBD to ScanSAR and ScanSAR to ScanSAR interferometry methods. We are very fortunate that there is one adequate interferometric pair spanning the Wenchuan earthquake. An accurate geometric model of the region enables recombination of interferometric swaths in the geographic coordinates.

Data and Methods

The InSAR data are from the L-band (23.6 cm) SAR aboard the ALOS spacecraft launched by JAXA in January, 2006. Data acquisition prior to the earthquake is generally excellent because of the global nature of the PALSAR background mission. The background mission collects strip-mode images along ascending orbits and ScanSAR images along descending orbits. Data are provided by JAXA through the Alaska Satellite Facility using funding from the National Science Foundation.

Pre-Processing

We use SIOSAR to process ALOS PALSAR data. Special ALOS preprocessing code has been written to read the CEOS headers and data, align the echos in range, compute the precise orbits, and to convert among the three main modes of operation, FBD (14 MHz), FBS (28 MHz), and ScanSAR (WB1 - 5 subswaths at 14 MHz). A layer-cake ionospheric correction has been developed using the global ionospheric model (GIM) developed at JPL http://iono.jpl.nasa.gov/gim.html. A subset of preprocessing code and documentation is available at http://www-rohan.sdsu.edu/~rmellors/ALOS_preproc.tar.gz.

Standard Swath Interferometry - Ascending Orbits

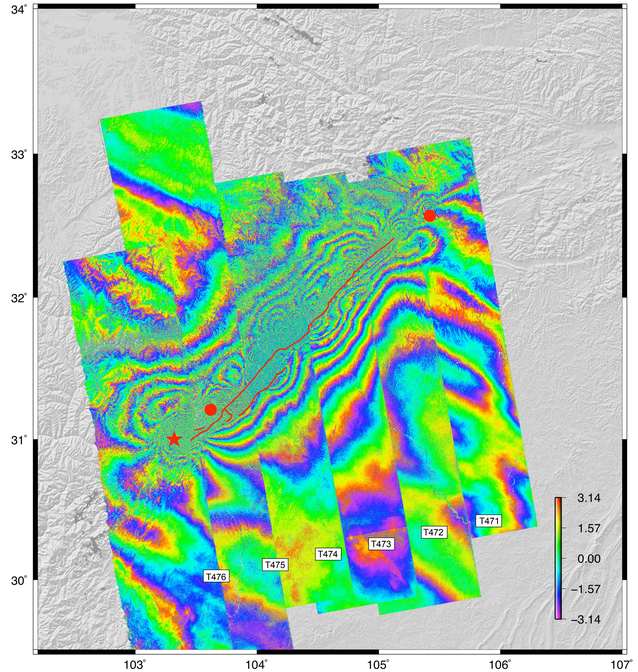

Fig 2. Ascending strip mode linterferograms (11.8 cm per fringe) from 78 scenes of ALOS PALSAR data. The red star is the main shock, the red circles are the magnitude 6 aftershocks on May 12th and May 25th. The red line is the surface rupture mapped by Jing Liu from the Chinese Academy of Sciences. While the lowland areas have good phase coherence, the phase recovery is decent in the mountainous areas. Lower coherence is due to a combination of extreme ground shaking, temporal decorrelation from vegetation, and inadequate topographic phase correction in the area of extreme relief.

Processing on Swath Interferometry

The highly accurate ALOS orbits (< 7 cm error), combined with the small Doppler centroid, simplifies the interferometric processing. The frames along each track (39 interferograms) are processed individually to improve image matching (i.e. smaller areas) and keep file sizes manageable. Individually-processed interferograms abut seamlessly for mosaicing in either radar or geographic coordinates. The phase mismatch between swaths has three possible causes: temporal variations in atmospheric and ionospheric delay, post-seismic deformation, and orbital error. Without additional analysis we have not been able to separate the sources of the error.

A plane is removed from each swath to minimize the phase ramps far from the rupture zone. Tracks 471, 475, and 476 have significant residual phase error perhaps due to ionospheric waves. Automatic phase unwrapping is difficult in the mountains and impossible along the fault zone. We visually connect fringes around the ends of the faults and digitize fringe counts. (Fig 3)

Table 1. Acquisition dates, baseline, planar trend of the phase of ascending track

Track	476	475	474	473	472	471
Dates	Apr 8, 2008 May 24, 2008	Jun 20, 2007 Jun 22, 2008	Mar 5, 2008 Jun 5, 2008	Feb 17, 2008 May 19, 2008	Jan 28, 2007 Jun 17, 2008	Feb 29, 2008 May 31, 2008
Baseline (m)	-197.1	-14.4	267.9	196.5	209.8	62.8
Plane sx	-3	-3	0	-6	6	-15
removed sy	-4	-6	0	0	12	-15
(rad/deg)						

Inversion for Coseismic Model

Both descending and ascending InSAR data constrain the distribution of coseismic slip based on an elastic half-space formulation [Okada, 1985] using the inversion code developed by Fialko [2004]. The decorrelation in mountains combined with shadowing and layover effect prevent automatic phase unwrapping. Our solution is to digitize the fringes manually and convert them to displacement in the line of sight direction. We subdivided Beichuan Fault into 3 segments according to geological surface measurement. Both Beichuan Fault and Penguan Fault planes are elongated beyond the surface rupture to capture the subsurface slip. We have examined the rms misfit versus dip angle and found the best fit models have fault dip between 45 and 55 degrees toward northwest. The geodetic moment is 9.63*10^20 N m which is equal to a seismoc moment magnitude of 7.92. The geodetic moment is nearly equally partitioned between dip-slip (6.02*10^20 N m) and strike-slip (5.87*10^20 N m).

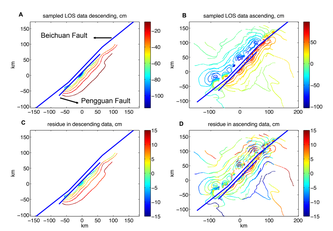

Fig 3. A) Sampled line of sight (LOS) data in descending track. Deformation on the west side of the fault is unavailable. B) Sampled line of sight (LOS) data in ascending track. Deformation reaches as far as 100km away from the fault zone. The deformation between Beichuan and Penguan fault is crucial to discriminate the slip partition, but unfortunately, they are not well recoverable by this dataset. C) Residuals after subtracting the best fitting models from the descending data. Note the color scales are different. For descending track, the residue has a mean value of 4.76 cm, and standard deviation is 6.09 cm. The non-zero mean apprears as a trend in the residue that need to be understood. D) Residuals after subtracting the best fitting models from the ascending data. For ascending track, the mean value of the residue is 0.31 cm, standard deviation is 6.53 cm. However, the misfit is worse at the northern end of Beichuan fault. Note the magnitude 6 aftershock occurred nearby the localiaztion of the residue.

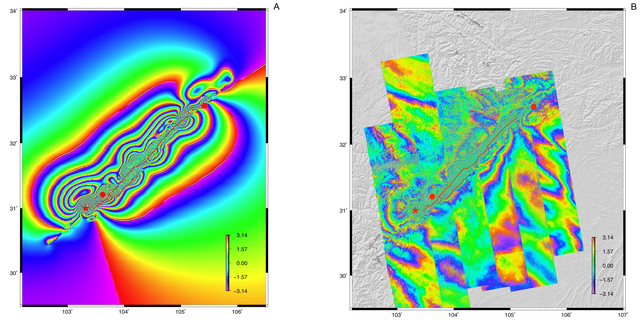

Fig 4. A) Synthetic interferogram derived from InSAR data with half-space elastic model. The red line shows the surface rupture. The red star and circles show the epicenter locations. Several features match well with the ascending interferograms in Fig 2. B) Residue interferogram obtained by subtracting the model from the phase data, then wrapping it again. The residue in track 471, 474, 475 are within one fringe. Note there are two fringes that can't be resolved by our simple model in the track 472 and 473. It's possible that our model need to account in the complex fault geometry in depth, with the aftershock relocation data.

Preliminary slip model

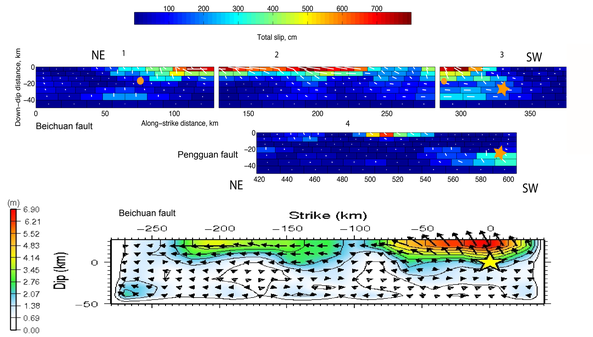

Fig 5. Above is our model based on InSAR data. Below is from seismic inversion. (Nishimura & Yagi, 2008) Star and circles show location of the main shock and two magnitude 6 aftershocks. Arrows show the slip direction of hanging wall relative to foot wall (right lateral, west side up) See Fig6. for numbers of the fault segments. Overall the InSAR and seismic models have similar patterns but the InSAR data resolve more of the details of the slip. Near the epicenter, the faulting is mainly dominated by dip component and the rupture reaches 10-20km in depth. Toward the northeast, the slip gradually transforms from dip-slip to strike-slip. At Beichuan fault, there is a reduction in slip between 240 and 280 km and a complimentary increase in slip on the nearby Pengguan fault. Looking at the difference, we find our model has generally larger slip magnitude, especially the strike-slip component in the northern part of Beichuan fault. In addition, the Penguang fault, which parallel to the major fault, is constrained to have shallower slip. There is slip motion of magnitude 3m in a depth of 30km, in both northern and southern part of our fault model. Whether it's real signal that reflect deeper slip during the earthquake, or artifacts is an interesting question. The teleseismic inversion retaining this feature is an encouraging sign. Dip angle is 45 degrees for Beichuan fault and 30 degrees for Pengguan fault.

Comparison between model predictions and GPS

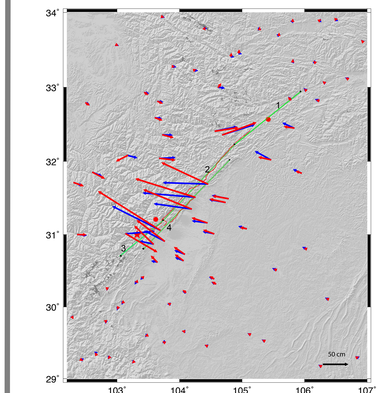

Fig 6. We compare the horizontal movement predicted by our model (blue) with the GPS measurement (red) by simulating the 3D displacement at the same position as the GPS site [Zhang, 2008]. In general, the data agree with our model predictions, but there may be a systematic inconsistance: our model indicate more strike-slip component while GPS data gives more dip-slip component, especially closer to the faults.

Conclusion

Radar Interferometry:

- L-band interferometry from ALOS has adequate correlation in vegetated and mountainous areas west of the rupture.
- ScanSAR-to-ScanSAR interferometry provides new deformation measurements along the descending track.
- The interferograms are completely decorrelated on the hanging wall side of the rupture suggesting the surface was disturbed by extreme shaking.

Elastic dislocation modeling:

- The slip model shows: dominant thrust (~6 m) in the epicentral area, shallow (< 8 km) strike-slip (~6 m) toward the northeast, and patches of deep slip (~20 km) at the ends of the ruptures.
- Total geodetic moment of Wenchuan earthquake is 8 times greater than that from Landers earthquake and in agreement with a 7.9 seismic moment magnitude. The moment of strike-slip is about equal to dip slip.
- Preliminary model based on InSAR data shows some systematic misfit with GPS measurements that will be investigated in the near future.